JACS
JOURNAL OF THE AMERICAN CHEMICAL SOCIETY
Article
pubs.acs.org/JACS

Hydrogen-Bond Dynamics of Water at the Interface with InP/GaP(001) and the Implications for Photoelectrochemistry

Brandon C. Wood,* Eric Schwegler, Woon Ih Choi, and Tadashi Ogitsu

Quantum Simulations Group, Lawrence Livermore National Laboratory, Livermore, CA 94550

Supporting Information

ABSTRACT: We investigate the structure, topology, and dynamics of liquid water at the interface with natively hydroxylated (001) surfaces of InP and GaP photoelectrodes. Using *ab initio* molecular dynamics simulations, we show that contact with the semiconductor surface enhances the water hydrogen-bond strength at the interface. This leads to the formation of an ice-like structure, within which dynamically driven water dissociation and local proton hopping are amplified. Nevertheless, the structurally similar and isovalent InP and GaP surfaces generate qualitatively different interfacial water dynamics. This can be traced to slightly more covalent-like character in the binding of surface adsorbates to GaP, which results in a more rigid hydrogen-bond network that limits the explored topological phase space. As a consequence, local proton hopping can give rise to long-range surface proton transport on InP, whereas the process is kinetically limited on GaP. This allows for spatial separation of individual stages of hydrogen-evolving, multistep reactions on InP(001). Possible implications for the mechanisms of cathodic water splitting and photocorrosion on the two surfaces are considered in light of available experimental evidence.

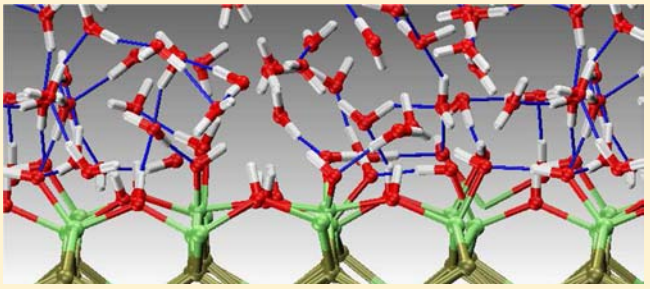

INTRODUCTION

Photoelectrochemical cells promise sustainable production of hydrogen from water using solar energy.[1] In these devices, photogenerated carriers are responsible for driving the water redox reaction at the interface between the semiconductor electrode surface and an electrolyte solution.[2−4] Of the available semiconductor electrode materials, polar surfaces of group-III phosphides currently show the highest reported hydrogen evolution activity; however, the durability of the electrode surfaces under operating conditions remains a significant impediment.[5−11] Efficient and stable operation of a photoelectrode material depends on several factors, including proper alignment of the band edges with respect to the redox potentials of water. These tend to be highly sensitive to the details of the semiconductor−water interface, which requires a fundamental understanding of how water affects and is affected by the surface states.[1,3]

Oxygen-derived adsorbates are known to appear on III−V surfaces, even after surface cleaning.[9,12−14] These inevitably modify the surface states, even prior to photoillumination.[8,14−19] For instance, the presence of native oxygen-derived adsorbates on Ga/In-rich GaP(001) and InP(001) fundamentally change the surface structure and chemistry when placed in contact with water.[20,21] This is primarily due to hydrogen-bonding interactions, which play an especially large role when liquid water is present. The surface modifications form the subject of a forthcoming paper from our group,[21] in which we investigated metal-rich GaP/InP(001) surfaces in contact with gas-phase and liquid water, considering both the pristine surface and formation of a submonolayer native surface oxide. The simulations suggested that the surface oxide would lead to dense surface hydroxylation on either surface. Evidence of surface hydroxylation was also observed in recent ultrahigh vacuum experiments on epitaxially grown mixed-dimer $\delta(2 \times 4)$ GaP(001).[22] Accordingly, hydroxyl-rich surfaces can be considered an appropriate model for studying the equilibrated interface of GaP/InP(001) with neutral-pH water.[21]

In this paper, we show how natively hydroxylated InP(001) and GaP(001) modulate the hydrogen-bond network structure of interfacial water in qualitatively different ways, despite the fact that the two surfaces are isovalent and have nearly identical surface structures. This is particularly surprising in light our report that the structure and chemistry of water-exposed surface adsorbates on the two species are very similar.[21] The origin of the differences can be traced to subtly different chemistry of the metal−oxygen bonds, which impacts hydrogen-bond strength and dynamics not just for surface-adsorbed water, but throughout the first few water layers. The disparity in the interfacial hydrogen-bond network dynamics has broad implications for transport behavior, which in turn provides a possible interpretation of macroscopically observable experiments on GaP and InP electrodes for photoelectrochemical hydrogen production. They also offer a fundamental study of how small differences in model hydrophilic surfaces can

Received: April 17, 2013
Published: September 20, 2013

   dx.doi.org/10.1021/ja403850s | J. Am. Chem. Soc. 2013, 135, 15774−15783

modulate interfacial water structure and chemistry in unexpected ways.

COMPUTATIONAL DETAILS

Car–Parrinello molecular dynamics simulations[23] were run within the canonical *NVT* ensemble using the Quantum-ESPRESSO code.[24] A fictitious electronic mass of 700 au and a time step of 12 au were used. Deuterium was substituted for hydrogen to permit the larger values. Accordingly, the term "hydrogen" should be assumed to refer to deuterium throughout the text. Ultrasoft pseudopotentials[25] were used for all elements, and semicore *d* states were included in the valence descriptions for indium and gallium. Cutoffs of 30 and 300 Ry were used for the wave functions and charge density, respectively. The Perdew-Burke-Ernzerhof (PBE) exchange-correlation functional[26] was adopted for suitable description of the hydrogen bonds.[27]

The semiconductor–water interface was generated using seven semiconductor layers oriented along (001), with periodic boundary conditions imposed. A (4 × 4) supercell with cell axes aligned along [110] and [$\bar{1}$10] was generated, with top and bottom layers identically terminated to minimize spurious interactions between periodic images. The In-/Ga-rich surface was used, since this termination is the most favorable for oxygen adsorption[18] and is therefore likely to exhibit surface hydroxylation.[21] A total of 1.65 nm of liquid water was included, enough to approximate the ambient density of liquid water at the point farthest from the two surfaces. In total, the initial supercell configuration consisted of 112 semiconductor atoms, plus 48 surface-adsorbed hydroxyl groups and ∼160 water molecules.

In order to select a suitable model for surface hydroxylation of InP(001) and GaP(001), we relied on low-energy configurations and coverages from our previous stability analysis,[19] as well as our studies of the products of water dissociation on oxygen-rich surfaces.[20,21] The models were constructed by combining surface *M*–[OH]–*M* bridges along [$\bar{1}$10] with *M*–OH dangling bond atop structures (1.5 ML coverage). Details of the initial surface configuration, along with the procedure used to equilibrate the interface prior to the production runs, can be found in the Supporting Information.

RESULTS AND DISCUSSION

Network Formation and Composition. Water adsorption on InP(001) or GaP(001) in the presence of surface oxygen or hydroxyl leads to the formation of interfacial hydrogen bonds.[20,21] Within the resulting surface O–H···O complexes, the weakening of the O–H chemical bond and strengthening of the O···H hydrogen bond results in low barrier for Grotthuss-type local proton transfer,[28] which we were able to observe in the full dynamics of oxygen-adsorbed InP/GaP(001) in contact with liquid water.[20,21] Similar local proton-hopping behavior has been theorized or observed in the context of several other interfacial systems.[29−38]

Here, we report that local proton-hopping mechanisms analogous to those reported for oxygen-adsorbed GaP/InP(001)–water interfaces in ref 21 are also observed at the interface with the hydroxylated surface. Whereas a bridge oxygen is the proton acceptor in the former, the latter features an atop hydroxyl group (*M*–OH) as the proton acceptor. The reactions proceed either by direct proton transfer from a water molecule adsorbed on a neighboring In/Ga site, or else by proton transfer across a Grotthuss chain that involves one or more liquid water molecules and an H_3O^+ transition state. The net result in this case is the formation of a new water molecule at a different surface site, which conserves the total number of water molecules. Schematically, the observed proton-transfer reactions to a bridge oxygen site (from ref 21) and to an atop hydroxyl site (based on this work) can be expressed as follows:

$$M\text{–}OH_2 + M\text{–}O\text{–}M \leftrightarrow M\text{–}OH + M\text{–}[OH]\text{–}M \quad (1)$$

$$M\text{–}OH_2 + M\text{–}OH \leftrightarrow M\text{–}OH + M\text{–}OH_2 \quad (2)$$

Because an atop *M*–OH complex is both a product of the forward reaction of eq 1 and a reactant in the forward reaction of eq 2, dissociation products may promote further dissociation.[21] Eventually, under sufficiently dense adsorbate coverage, the surface will nucleate the formation of a well-defined interfacial hydrogen-bond network. In practice, thermal fluctuations and reversible local proton transfer create a dynamic equilibrium with the solvent environment. Accordingly, component surface structures may include bridge oxygens and molecular water, in addition to hydroxyl groups. The average surface concentrations of each will be dictated by the equilibrium interfacial properties, modulated by external factors such as pH.

In order to identify and map the component structures involved in hydrogen bonding, we examine the individual spatial densities of oxygens with different numbers of attached protons in Figure 1. In this way, we can distinguish between O,

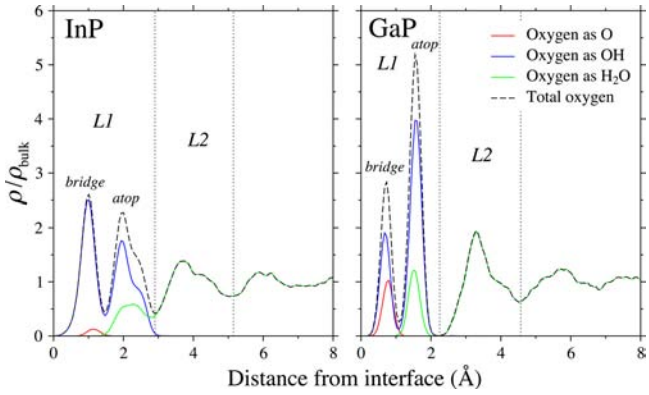

Figure 1. Density of O, OH, and H_2O moieties as a function of distance from the first full In-/Ga-rich layer in hydroxylated InP/GaP(001). The total density of oxygen is shown as a dashed line. Boundaries for the *L*1 and *L*2 regions are delineated by dotted lines.

OH, and H_2O at the interface. Looking first at the overall density of oxygen as a function of distance from the interface, we isolate two regions of particular interest for further analysis. The first region (*L*1) represents the surface adsorbate layer, which can be further decomposed into bridge and atop configurations by noting their direct correspondence with the first two sets of oxygen-derived peaks in Figure 1. Categorizing atop and bridge bonds separately enables us to confirm that a lone surface oxygen occurs uniquely as a bridge bond (*M*–O–*M*), water as an atop bond (*M*–OH_2), and hydroxyl as either configuration (*M*–[OH]–*M*, *M*–OH). The second region (*L*2) is the first interfacial solvent layer, in which nearly all oxygens exist as water molecules. Although we focus our analysis on the *L*1/*L*2 region, we point out that clear fluctuations in the oxygen density are observable beyond the *L*2 boundary. This underscores the value of accounting for the full solvation environment in lieu of a simpler model based only on a *L*1–*L*2 water bilayer.

A well-defined boundary exists between *L*1 and *L*2 in Figure 1. This is similar to the behavior reported for other hydrophilic systems, including SiC(001)[39] and TiO_2.[40] However, the boundary is noticeably more pronounced for GaP than for InP. In fact, we calculate zero oxygen density in the *L*1/*L*2 boundary region of GaP, meaning water molecules are *never* observed to exchange between the surface adsorbate layer and

dx.doi.org/10.1021/ja403850s | J. Am. Chem. Soc. 2013, 135, 15774−15783

the solvent, once the interface has equilibrated. In contrast, the $L1/L2$ interface for InP appears to be much more fluid.

Similarly, the gap between the atop and bridge hydroxyl peaks of $L1$ in Figure 1 has a much deeper minimum for GaP than for InP. The region between these peaks represents the transition state between the atop and bridge bond types, which occurs by breaking or forming one of the $M-$OH bonds in the bridge. Accordingly, we infer that topological interchange of atop and bridge hydroxyls is much less frequent for GaP. This is examined more fully in the next section. The $L1$ and $L2$ layers are also much narrower for GaP than for InP, as are the distributions of oxygen density within each layer. Together, these features support the interpretation of a more rigid, well-defined network structure at the interface with GaP.

Within $L1$, where the identity of the surface species varies, we can integrate over the peaks in Figure 1 to obtain the relative likelihood of the bridge oxygen ($M-$O$-M$), atop hydroxyl ($M-$OH), bridge hydroxyl ($M-$[OH]$-M$), and atop water ($M-OH_2$) bond types. The normalized fractions of each type are shown in Table 1. We have also translated these values into estimated differences in free energy ΔF at the given simulation temperature, assuming the system is in equilibrium.

Table 1. Relative Populations p of Oxygens in the $L1$ Region of InP/GaP(001) Belonging to the Four Dominant Surface Oxygen-Containing Bond Types

bond type	p on InP (%)	ΔF on InP (meV)[a]	p on GaP (%)	ΔF on (meV)[a]
$M-$O$-M$	1.7	+109	11.8	+51
$M-$[OH]$-M$	40.5	+0	21.8	+30
$M-$OH	39.5	+1	51.4	+0
$M-OH_2$	18.2	+28	15.1	+42

[a]Estimated free energy differences are calculated with respect to the highest-concentration bond topology according to $\Delta F = -k_B T \ln (p_1/p_2)$.

On the basis of the $L1$ concentrations in Table 1, it is immediately evident that the $M-$[OH]$-M$ bridge and the atop $M-$OH comprise the primary building blocks of the hydrogen-bond network at the surface. However, bridge oxygens and atop water molecules also appear in non-negligible concentrations. The importance of the solvent is implicit in the results: the computed free energy differences of the bond topologies in Table 1 have a spread that is much smaller than the reported spread of zero-temperature energies in the absence of liquid water[19] (10s of meV, rather than 100s of meV). For example, consider that the zero-temperature formation energy of an $M-$[OH]$-M$ bridge at the vacuum interface is lower than that of an atop $M-$OH by 510 meV (300 meV) for InP (GaP) when averaged over unique surface configurations in ref 19. Nevertheless, when the finite-temperature solvent is included, the atop $M-$OH features prominently, and the free-energy difference becomes very small. This means that the degree of solvent-driven stabilization depends on the bond type. In the case of atop hydroxyl, preferential stabilization is likely traceable to increased favorability for hydrogen bonding. This follows from the atop hydroxyl being able to accept an additional hydrogen bond, as well as its having less steric hindrance.

This apparent flatness of the free energy landscape (Table 1) is aided by opposite heuristic trends in the solvation and formation energies. Relying on the formation energies calculated in ref 19 and ignoring interactions between adsorbates or with a solvent, the general order of surface adsorbate stability is $-$[OH]$-$ > $-$OH $\geqslant$ $-$O$-$ > $-OH_2$. If we use the number of possible hydrogen bonds with the solvent as an indicator of the solvation energy, this order is essentially reversed: $-OH_2$ (2 donors, 1 acceptor) > $-$O$-$ (0 donors, 2 acceptors) = $-$OH (1 donor, 1 acceptor) > $-$[OH]$-$ (1 donor, 0 acceptors). The competition between formation and solvation energies makes all four topologies realizable in the simulations, although changes in pH and temperature will shift reaction equilibria to favor formation of certain complexes over others.

Interestingly, significant differences are seen when comparing GaP and InP in Table 1, which are signatures of fundamentally different network compositions. For instance, in the case of InP, the bridge and atop topologies appear with near-equal likelihood, whereas for GaP, there is more than a two-to-one preference for atop $M-$OH. This may be a factor in the more rigid network for GaP in the $L1$ region, since atop hydroxyls can also accept hydrogen bonds and generally interact more strongly with the $L2$ solvent layer due to proximity. Another difference is that the relative likelihood of finding lone surface bridge oxygens not bonded to protons is nearly six times greater for GaP than for InP. This suggests that GaP more readily donates protons to the solution, and has a higher pK_a. The different surface concentrations of lone bridge oxygens has possible implications for corrosion mitigation if these bridges contribute to photocorrosion via hole trapping, as we have previously postulated.[19]

Network Connectivity and Topology. In this section, we discuss the static and dynamic topology of the hydrogen-bond network. This provides insight that is not contained explicitly in the time-averaged structure in Figure 1. For instance, a topological map has the capability to distinguish between hydrogen bonds formed within a layer, bonds formed to the next outer layer, and bonds formed to the next inner layer. Accordingly, we have calculated a full spatial density map of hydrogen bonds, resolved by location of both donor and acceptor oxygens, shown as planar-averaged density contours in Figure 2a,b. We have also performed a similar analysis for the density of hydrogen-bond breaking (Figure 2c,d), which gives a measure of which types of hydrogen bonds are likely to break or remain intact. In discussing Figure 2, we reintroduce the notation $L1$ and $L2$ to refer to the adsorbate and first solvent layer, respectively. Within $L1$, we additionally distinguish between bridge bonds ($L1$-*br*) and atop bonds ($L1$-*at*).

The local maxima in a and b of Figure 2 represent the most frequent donor–acceptor combinations for InP and GaP. As expected, hydrogen bonds between $L1$ (bridge and atop) and $L2$ are common (labeled *A* and *B* in the figure). Bonds between two $L1$-*at* oxygens are also common (labeled *C* in the figure), particularly for GaP. Overall, however, InP features a larger number of local maxima, indicating greater variety in the types of hydrogen bonds that can be formed. For instance, InP shows hydrogen bonding between $L1$-*br* and $L1$-*at*, and even directly between two $L1$-*br* bridges.

A comparison of the overall hydrogen-bond density contours (Figure 2a,b) with the density contours of hydrogen-bond breaking (Figure 2c,d) reveals some additional surprises. For instance, hydrogen bonds from $L1$-*br* to $L1$-*at* break most frequently for InP, despite the fact that the $L1$-*br* → $L1$-*at* bond is not a particularly prevalent bond type. For GaP, $L1$-*at* → $L1$-*at* bond breaking entirely dominates, but to an even greater

dx.doi.org/10.1021/ja403850s | J. Am. Chem. Soc. 2013, 135, 15774–15783

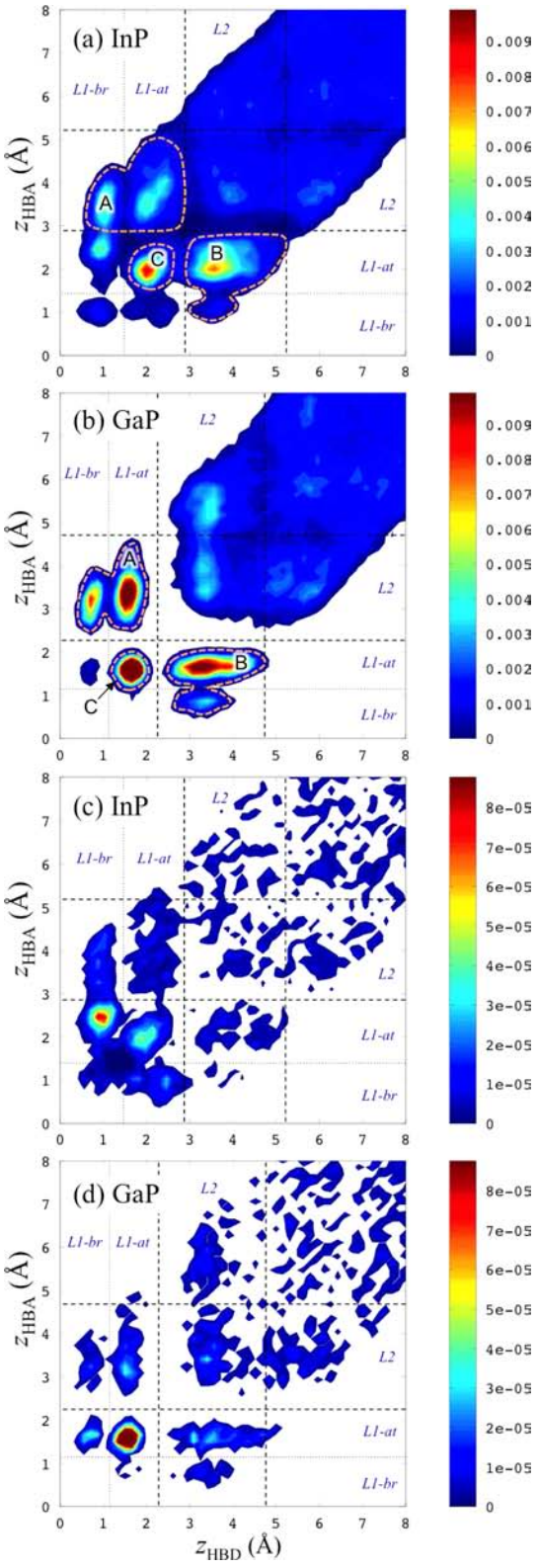

Figure 2. Planar-averaged density contours (Å^{-3}) of hydrogen bonds, indexed by the position z of the hydrogen-bond donor (HBD) and acceptor (HBA) oxygens, measured perpendicular to the interface. Panels (a) and (b) show the overall hydrogen-bond density for InP and GaP, respectively; (c) and (d) show the density of hydrogen-bond-breaking events. White space means zero density. *L1-br* and *L1-at* refer to the bridge and atop peaks in Figure 1.

degree than one might expect from an examination of the overall density contours. This likely relates to the especially high rate of proton exchange between neighboring *L*1−*at* atop groups that we observe for GaP,[21] which simultaneously breaks hydrogen bonds. We also observe significantly enhanced hydrogen-bond density for GaP between two *L*2 oxygens, as well as from *L*2 oxygens to oxygens farther from the interface. Both features have a relationship to the oxygen density peak in the *L*2 region of Figure 1. In addition, both surfaces feature higher densities of hydrogen-bond breaking near the interface than in the bulk-like region (Figure 2c,d). This indicates that the network dynamics at the interface are in general faster than in the bulk liquid.

The area of phase space that is spanned by each of the local wells in Figure 2 is physically related to the rigidity or fluidity of the corresponding hydrogen-bond network component. Comparing the contour maps for InP (Figure 2a) and GaP (Figure 2b), it is immediately evident that the potential energy surface for hydrogen bonds, as parametrized by donor and acceptor position, is substantially flatter for InP than for GaP. This is clear from the sharpness of the peaks in the density profile of GaP, as well as the generally smaller area of phase space that is associated with each. This implies that the hydrogen-bond network in the interfacial region is significantly more structured and rigid for GaP, similar to what we concluded based on Figure 1. Some structure is even observable in the density of GaP *L*2 oxygens donating hydrogen bonds to layers farther from the interface.

The frequented regions of phase space in the interfacial region (bonds involving only *L*1 and *L*2 donors and acceptors) in Figure 2 are largely disconnected in the case of GaP but are continuous for InP. Connectedness is related to the capability of the hydrogen-bond network to interchange between topologies. This can happen in one of two ways: either the oxygen donor/acceptor migrates between layers (keeping the network otherwise intact), or else a hydrogen bond of one topology is broken and then reformed to an oxygen with a different topology. Within the interfacial region, there is some minor continuity between regions corresponding to *L*1 bridge and *L*1 atop donors/acceptors for GaP. This is an artifact of the interchange between bridge and atop hydroxyls, described earlier in the context of Figure 1, and shows up less prominently than for InP. Otherwise, any hydrogen-bond-breaking and adsorbate reorganization events in the interfacial region of GaP occur only within their originally defined interfacial layer. This behavior is in sharp contrast to InP, which demonstrates continuity between nearly all regions of the interfacial hydrogen-bond configurational phase space. This means hydrogen bonds at the InP/water interface, in addition to their host oxygens, are being continually and fluidly exchanged between layers. The topological fluidity of InP over GaP is also clear in the hydrogen-bond-breaking contour map (Figure 2c,d).

The surface dynamics of GaP and InP offer insight into the underlying reasons for the different fluidities of the interfacial hydrogen-bond networks. Two likely contributions are illustrated in Figure 3. The first relates to the enhancement of the hydrogen-bond strength of *L*1 donors, which turns out to be larger for GaP than for InP. We can see this in Figure 3a, which plots the vibrational density of states (VDOS) of hydrogens in *L*1, as calculated by taking the Fourier transform of the velocity autocorrelation function. Here we have focused on the librational modes about hydrogen bonds, which

dx.doi.org/10.1021/ja403850s | J. Am. Chem. Soc. 2013, 135, 15774−15783

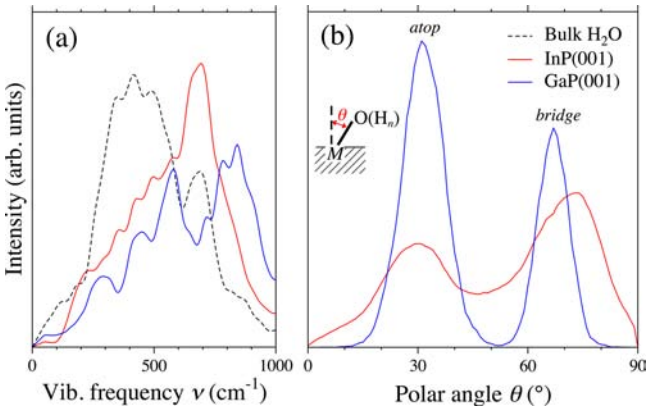

Figure 3. (a) Vibrational density of states (VDOS) for hydrogen atoms in the *L*1 interfacial region of OH-adsorbed InP(001) and GaP(001), compared with atoms in the bulk-like water region farthest from the periodic surface images. (b) Distribution of the orientation of *M*−O bonds on OH-adsorbed InP(001) and GaP(001), measured as the polar angle with respect to the surface normal direction.

dominate the spectrum below 1000 cm^{-1} and are a good indicator of hydrogen-bond strength and rigidity. The spectrum shifts toward higher frequencies when compared with the bulk-like water region, indicating stronger hydrogen bonds for both surfaces. However, the shift is noticeably larger in the case of GaP, in agreement with its observed rigidity.

The second factor relates to the softness of the In-derived surface modes, and to the corresponding strength and covalency of the Ga−O bond with respect to the In−O bond.[19] This is illustrated in Figure 3b, which shows the orientations of *M*−O bonds at the surface, measured with respect to the surface normal. The distribution is bimodal, with low- and high-angle peaks corresponding to component atop (*M*−OH) and bridge (*M*−[OH]−*M*, *M*−O−*M*) structures, respectively. The distribution for InP is much broader than for GaP, indicating higher-amplitude oscillations. According to Figure 3a, these oscillations are also lower in frequency, indicating a softer and more fluid surface. Note that the low likelihood of intermediate angles for GaP in Figure 3b translates to fewer interchanges between atop and bridge structures, consistent with our analysis of Figures 1 and 2.

We can quantify the range of topological phase space spanned by the hydrogen-bond network dynamics by introducing an index that measures the diversity of hydrogen-bonding configurations across simulation frames. To do so, we first introduce the adjacency matrix **A** to map the topology of the hydrogen-bond network within a directed graph-theoretic formalism.[41] Oxygens in the system are indexed {1,...,*N*}, and the element A_{ij} of the $N \times N$ adjacency matrix is defined as one if oxygen *i* donates a hydrogen bond to oxygen *j*, and zero otherwise. Within this scheme, we can define a *diversity index D* of the explored phase space as follows:

$$D = \exp\left(-\sum_{ij}^{N} \langle \mathbf{P}_{ij} \rangle \ln \langle \mathbf{P}_{ij} \rangle\right) \quad (3)$$

where

$$\langle \mathbf{P}_{ij} \rangle = \frac{\langle \mathbf{A}_{ij} \rangle}{\sum_{ij}^{N} \langle \mathbf{A}_{ij} \rangle} \quad (4)$$

Here we have used angle brackets to denote averages over equilibrated simulation frames. We applied the definition in eq 3 separately to the donor−acceptor pairs within each interfacial region (e.g., *L*1 or *L*2) by including only those pairs in the calculation of $\langle \mathbf{A}_{ij} \rangle$.

Equation 3 is directly derived from the Shannon entropy in information theory, which measures the self-information content of a data set (see ref 42 for details). Roughly speaking, *D* is related to the minimum number of state variables required to uniquely describe the topology of the hydrogen-bond network. Physically, it relates both to the size of the topological phase space explored during the simulation, and to the uniformity of that phase space exploration. *D* will trend toward smaller values for networks of low topological diversity (sparse, nonuniform ***A***) and larger values for networks of high topological diversity (dense, uniform ***A***). The definition of *D* is advantageous in that it maps the efficiency of phase space exploration not only between successive interfacial layers, but also *within* each layer.

Table 2 shows the computed values of *D* for all combinations of hydrogen bonds donated and accepted by the *L*1 or *L*2 regions. As expected, InP shows significantly higher topological diversity. This confirms that the topological phase space explored by the interfacial hydrogen-bond network of InP is much broader than for GaP, and that the exploration is relatively efficient and uniform across topological configurations.

Table 2. Calculated Values of *D* for Oxygen Donor/Acceptor Combinations in the *L*1 and *L*2 Interfacial Regions of Hydroxylated GaP(001) and InP(001)[a]

bond type	InP(001)	GaP(001)
*L*1 → *L*1	68	15
*L*1 → *L*2	67	31
*L*2 → *L*1	46	32
*L*2 → *L*2	104	48

[a]For reference, the computed value of *D* in the bulk-like water region is 324.

According to Table 2, the largest average difference between GaP and InP is seen for bonds wholly within *L*1. In this case, the value of *D* for GaP is particularly low, implying that the system shows very little topological variability. This is likely an artifact of the rigid atop−atop bonds for GaP, where repeated proton transfer induces hydrogen-bond breaking with very limited exploration of the phase space (see Figure 2d). Significant differences between GaP and InP are also seen for *L*1 → *L*2 and *L*2 → *L*2 bonds. This means that GaP is poor at exchanging hydrogen bonds and water molecules between the surface network structure and the solvent, whereas InP does so with much greater ease.

Network Dynamics and the Role of the Solvent. The previous sections have focused largely on characterizing the time-averaged properties of the hydrogen-bond network. We turn now to a schematic overview of the reaction mechanisms for hydrogen-bond forming and breaking near the interface, information about which is implicitly contained in the average contours of Figure 2. These reactions are typically connected to motifs in the hydrogen-bond network that topologically connect In/Ga surface atoms. These motifs involve *L*1 surface adsorbates of the types shown in Table 1 as well as *L*2 solvent molecules, and comprise the key building blocks for the

dx.doi.org/10.1021/ja403850s | J. Am. Chem. Soc. 2013, 135, 15774−15783

continuous, quasi-2D network that exists at the interface. They also form the backbone within which the local proton-transfer reactions in eqs 1 and 2 take place.

We begin by considering only those composite structures derived from surface hydroxyl groups in $L1$ (bridge and atop), since these occur with the highest frequency and exhibit the most diverse topologies. Direct inspection of the network dynamics allows us to identify four unique classes of hydroxyl-based component superstructures that topologically connect surface In/Ga atoms: hydrogen bonding between adsorbates; shared hydrogens in a Zundel-like structure; Grotthuss chains involving $L2$ solution molecules; and direct bridging with a single adsorbate. Examples representing each class are shown in the lettered diagrams of Figure 4. For complexes *a* and *c*, the

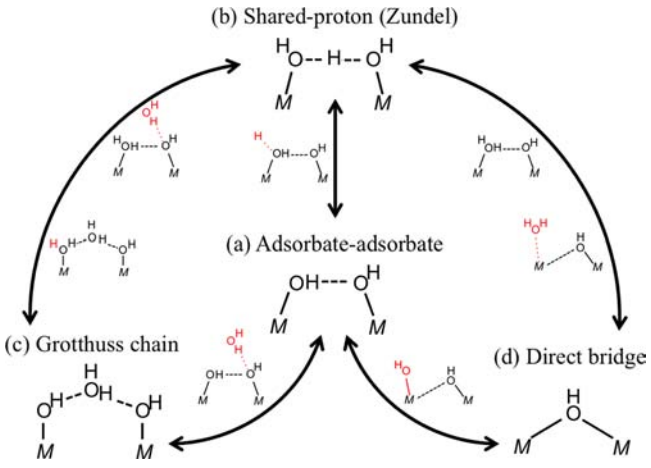

Figure 4. Schematic illustrations of four hydroxyl-involving surface configurations that bridge neighboring M sites, found in the course of the dynamics simulations of InP/GaP(001). Mechanisms by which the InP surface interchanges these configurations are shown alongside the arrows, with the red atoms coming from $L2 \rightarrow L1$ (solvent layer–adsorbate layer) exchanges. These exchanges are allowed for InP but kinetically inhibited for GaP.

atop hydroxyls are often substituted by bridge hydroxyls oriented into the plane of the paper. Complexes *c* and *d* occur preferentially along [110] and [$\bar{1}$10], respectively, which suggests that network reorganization and proton transfer behavior may not be isotropic. Note that structures analogous to those in Figure 4 have been reported on other hydrophilic surfaces following water dissociation, including oxides,[34,43,44] metals,[36] and III–V semiconductors.[37,45]

The difference in fluidity of the GaP and InP hydrogen-bond networks becomes especially relevant when considering possible interconversion between the four types of complexes shown in Figure 4. As a general rule, interconversion requires dynamic exchange of H, OH, or H_2O between the surface ($L1$) and the solvent ($L2$) environments (examples of solvent exchange reactions for InP are shown in Figure 4). Given that $L1 \leftrightarrow L2$ interlayer solvent exchange is rare (or forbidden) at the structurally rigid GaP–water interface, such interconversion reactions are observed only in simulations of the more fluid InP network.

As already discussed, the hydroxyl elements in Figure 4 may be dynamically converted into surface oxygen or water via local proton transfer. In this case, an atop hydroxyl (M–OH) accepts a proton (Brønsted–Lowry base) to become surface-adsorbed molecular water (M–OH_2), and a bridge hydroxyl (M–[OH]–M) donates a proton (Brønsted–Lowry acid) to become a bridge oxygen (M–O–M). This type of local proton transfer need not involve solvent exchange, and is therefore not forbidden by the comparatively rigid structure of the GaP–water interface. Rather, the rigidity of the GaP network statistically enhances local proton transfer, with local O–H bond-breaking events occurring roughly twice as frequently for GaP as for InP. This is likely due to a combination of longer average lifetime of highly aligned Grotthuss chains for GaP (Figure 4c), as well as a decreased exchange barrier due to stronger average hydrogen bonding.

The kinetics of hydrogen-bond network reorganization and local proton transfer appear to be in competition: the fluid network of InP favors the former, while the rigid network of GaP favors the latter. Nevertheless, InP still exhibits relatively facile site-to-site hydrogen transfer events, whereas GaP shows extraordinarily limited network reorganization capability and kinetics, especially within $L1$. In this regard, InP strikes a more favorable balance between the two factors. Accordingly, one should expect that local proton hopping should translate to rapid, long-range surface hydrogen transport on InP(001), provided adsorbate concentration becomes high enough to topologically connect the surface hydrogen-bond network. In contrast, local proton hops on GaP will be confined to a small region of phase space, preventing facile long-range transport. This is an instance in which minor differences in surface electronic structure generate qualitatively different macroscopic behavior.

The high observed frequency of interfacial chemical- and hydrogen-bond breaking, combined with the efficiency of the topological phase space exploration (Figure 2), point to significantly enhanced proton conduction within the $L1$ and $L2$ regions of the InP(001)–water interface. We note that similarly enhanced proton conduction with respect to bulk water has been documented for hydroxylated SiO_2.[44,46,47] Possible implications of this enhancement are discussed in the next section.

To identify what environmental factors motivate surface proton transport in the InP(001) simulation, we isolated frames in which a surface-adsorbed water molecule is undergoing dissociation. The local surroundings of the dissociating water were then analyzed and compared with intact surface-adsorbed water. We found a clear correlation between decreased distance to the nearest solvent water molecule and propensity for dissociation, as shown in Figure 5. Notably, the shortened water–water intermolecular distance appears prior to the dissociation event itself: the distribution in Figure 5 remains qualitatively unchanged if we examine frames up to 50 fs prior to O–H bond breaking. This means that instantaneous solvent environments featuring unusually close intermolecular water distances (shortened by ~0.3 Å) are significantly more likely to induce hydrogen transport. A similar correlation exists for Grotthuss diffusion in liquid water, which is likewise controlled by fluctuations in the instantaneous local network structure.[28] Repeating the analysis of Figure 5 for the nearest surface indium atom did not reveal any structural correlation. Accordingly, the surface may weaken the O–H bond, but it is the solvent environment which is most important at determining proton hopping.

■ POTENTIAL IMPLICATIONS

We begin by summarizing our results on the different dynamical properties of the InP(001)–water and GaP(001)–

dx.doi.org/10.1021/ja403850s | J. Am. Chem. Soc. 2013, 135, 15774–15783

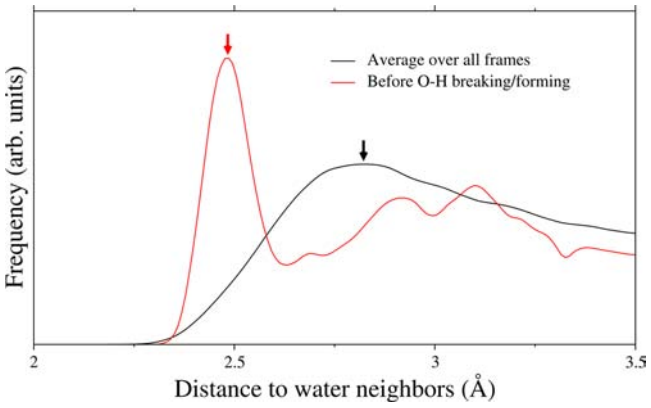

Figure 5. Distribution of oxygen−oxygen distances between adsorbed water (*L*1) on InP(001) and neighboring water molecules in solution (*L*2). The red line is for interfacial water molecules that break or form O−H bonds (forming OH^- or H_3O^+), sampled 10 fs prior to the bond-breaking/-forming event. The black line is averaged over all remaining frames. Arrows indicate the first density peak.

water interfaces, once native surface hydroxylation has been taken into account. Driven by the water-dissociation and proton-transfer reactions in eqs 1 and 2, the hydroxyl adsorbate concentration on both substrates will increase in the presence of surface oxygen until a well-defined hydrogen-bond network is formed, and the interface enters a dynamic equilibrium with the solvent environment. However, the nature of this equilibrium differs significantly between GaP and InP, as evidenced by the different average surface compositions (Table 1). It is also evident in the dynamical fluctuations among different compositions and topologies, which tend to be much greater for InP. Both surfaces exhibit rapid surface hydrogen transfer between nearby In/Ga sites, aided by a weakening of O−H chemical bonds and a strengthening of O···H hydrogen bonds at the interface. However, for GaP(001), the dynamics of surface hydrogen is largely limited to frequent local hopping events, due to the kinetic barriers associated with reorganization of the stiff interfacial hydrogen-bond network. On the other hand, InP(001) exhibits facile, solvent-driven network reorganization and rearrangement (Figures 2 and 4). The InP(001)−water interface is therefore characterized by fluid, collective surface hydrogen transport, as well as continual exchange of H/OH/H_2O with the solvent. In the following sections, we re-examine the differences between GaP and InP in view of their use as photoelectrochemical electrodes, as manifested in the hydrogen evolution and photocorrosion reactions.

Kinetics of Hydrogen Evolution. We use our results to speculate about the probable kinetics of the overall hydrogen evolution reaction (HER), including which steps are likely to be rate limiting. Our discussion is framed in the more specific context of the Volmer/Heyrovsky/Tafel process (eqs 5, 6, and 7), which is generally thought to underlie electrochemical hydrogen evolution.[48] In this model, the Volmer process (eq 5) first transfers an electron to an adsorbed proton. The reaction then proceeds either via the Heyrovsky process (eq 6) or the Tafel process (eq 7). In the Heyrovsky process, a proton is donated from the solvent to an adsorbed hydrogen atom, which is coupled to an electron transfer reaction to form H_2. In the Tafel process, two adsorbed Volmer hydrogens combine via surface diffusion to form H_2.

$$H^+_{(aq)} + e^- \rightarrow H_{(ads)} \quad (5)$$

$$H^+_{(aq)} + H_{(ads)} + e^- \rightarrow H_2 \quad (6)$$

$$2H_{(ads)} \rightarrow H_2 \quad (7)$$

In the context of the Volmer/Heyrovsky/Tafel process, the capability for fast surface proton transport has two potential benefits. First, it could lower the barrier for a purely transport-limited process—notably, the surface diffusion of hydrogen atoms as a precursor to the Tafel step (eq 7). Second, it could permit the H_2 formation site to be spatially separated from the Volmer site. This will be advantageous for either the Heyrovsky (eq 6) or Tafel (eq 7) processes if the kinetics of H_2 formation is site dependent, and more favorable away from the Volmer site.

On the pristine surface (without a surface catalyst), H_2 formation probably occurs via the Heyrovsky process (eq 6), as is common for semiconductors when unaided electron transfer is relatively inefficient.[49,50] In this case, the rate-limiting step at the semiconductor surface will be the proton-coupled electron transfer from the solvent to the hydrogen adsorbate. Enhanced surface conductivity would therefore probably not play a role.

However, metal surface catalysts are generally deposited on III−V photocathodes to enhance reaction kinetics.[5,15,51,52] It is known that the catalyst lowers the onset potential of the HER,

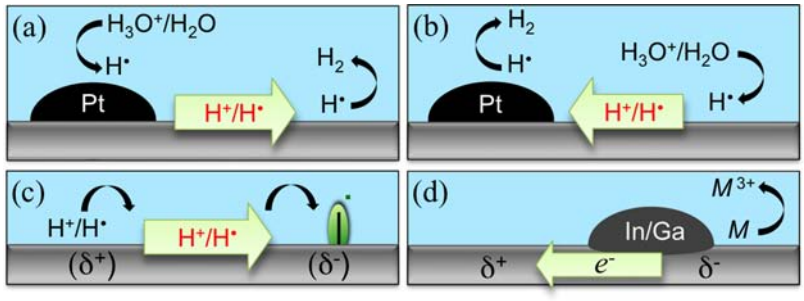

Figure 6. (a−b) Possible additional HER reaction mechanisms on InP(001), activated by surface hydrogen transport when an efficient Pt electrocatalyst is present. In these mechanisms, subsequent steps of the HER are spatially separated, with the catalyst improving the kinetics of either (a) the Volmer reaction (eq 5; Mechanism B in the text) or (b) the Tafel/Heyrovsky reaction (eqs 6 and 7; Mechanism C in the text). (c) Proposed self-healing mechanism on hydroxylated InP(001), in which a dangling bond (green) is passivated by the surface-diffusing species. The same proton-shuttling process can also charge-compensate for the buildup of a δ^+/δ^- potential difference arising from surface inhomogeneity. (d) Alternatively, charge compensation can occur via the competing mechanism of galvanic corrosion, in which electrons flow from ionized semiconductor atoms.

dx.doi.org/10.1021/ja403850s | J. Am. Chem. Soc. 2013, 135, 15774−15783

implying that it acts as a current collector for improved electron transfer kinetics.[15,53,54] This also leads to improved surface stability of Pt-decorated InP, since current is drawn away from carrier-trapping sites.[15,55] However, its role in each of the specific reaction steps of the HER at the semiconductor surface is less well understood.

A possible assumption is that all steps of the HER occur directly at the catalyst surface (Mechanism A). However, this appears to conflict with the fact that the Tafel slope of platinized *p*-InP(001) matches closely with the that of the uncatalyzed semiconductor but is very different from metallic Pt.[56−58] It is therefore likely that the semiconductor plays a more direct role in the HER mechanism. Accordingly, we also consider the possibility that the H_2 formation site can be spatially separated from the Volmer site. In this case, two other mechanistic possibilities emerge: the Volmer step could occur predominantly at the catalyst surface, with subsequent steps occurring on the semiconductor surface (Mechanism B), or else vice versa (Mechanism C). These latter two mechanisms are illustrated schematically in Figure 6a and 6b. If either one is relevant, then it is easy to imagine that surface proton transport on InP(001) would significantly enhance the HER reaction rate.

Let us first explore the possibility that the Volmer step (eq 5) occurs at the catalyst, but that subsequent steps (eq 6 and 7) occur on the semiconductor surface (Mechanism B). Notably, this is the same hydrogen spillover-assisted H_2 mechanism that was recently reported for a hydroxylated SiO_2/Si junction with a surface catalyst,[59] consistent with previous reports of a key HER step associated with hydrogen-bonded silanol at the semiconductor/solution interface.[60] On InP, Tafel slope measurements suggest that the Volmer step (eq 5) is probably rate limiting on pristine surfaces if no catalyst is present.[58] Because efficient electrocatalysts such as platinum tend to have low Volmer reaction barriers,[48,61] this supports Mechanism B. In this case, if surface hydrogen transport is kinetically inaccessible, as our simulations indicate is the case for GaP, then H_2 formation will be similarly confined to the catalyst site. On the other hand, on InP the adsorbed hydrogen might be transferred to the semiconductor surface, where it can diffuse to a low-barrier surface site for H_2 formation.

However, if the Volmer step (eq 5) is coupled to the dissociative adsorption of water (e.g., at high pH), then the barrier might be very different in the presence of native oxygen-derived surface adsorbates.[9,12−14,18] Specifically, the favorable kinetics of water dissociation on these sites (e.g., via eqs 1 and 2) means a metal surface catalyst would not be required for the Volmer stage. This supports the idea that the later stage of the HER are instead catalyzed by the metal, likely aided by a low hydrogen diffusion barrier on the catalyst surface[48] (Mechanism C). Here, surface hydrogen transport again becomes relevant. If it is kinetically accessible, as is apparently the case for InP, then adsorbed hydrogen from water dissociation at the oxidized semiconductor site can be shuttled to the semiconductor−catalyst interface. H_2 formation will then occur on the metal (e.g., via the Tafel process on Pt[48,61]).

If Mechanism B or C is correct, then our interpretation may help to explain why GaP does not show the same performance enhancement as InP upon addition of a platinum surface catalyst.[14,51] Our proposal is also consistent with various other established experimental results on InP. One of these is the improved performance of InP photocathodes in acidic electrolytes, where surfaces are more likely to be protonated and hydrogen-bond networks can form.[51,54,62] Similarly, it helps explain photovoltage improvements upon exposure of air-oxidized InP photocathodes to hydrogen-rich environments, as well as the reversal of such trends upon re-exposure to oxygen or application of positive potentials that strip away surface protons.[51,63,64] In addition, our proposal is consistent with the fact that increased areal catalyst density does not necessarily improve hydrogen evolution performance on InP.[15,51]

Corrosion. When a thin surface oxide is present, catalyzed InP has been shown to operate stably in an aqueous electrolyte.[7,15,17,62,65,66] However, oxidized GaP does not generally exhibit the same self-passivation behavior.[14] Similarly, decomposition products of the $GaInP_2$ alloy tend to be Ga-rich and In-poor.[9] The choice between the chemical pathways of corrosion/dissolution and passivation will depend on the thermodynamics and kinetics of the relevant processes during device operation. In this regard, we can extract clues from key differences between GaP and InP that we directly observe in the dynamics simulations.

First, the possibility of rapid, long-range surface hydrogen transport in InP(001) makes it especially easy to passivate any dangling-bond surface states with hydrogen. This is because the hydrogen does not need to be provided directly at the dangling-bond site, but can instead be quickly shuttled from any available reaction site. This offers a possible self-passivating mechanism by which the InP surface could heal itself, as shown in Figure 6c. Our results suggest that this same mechanism would not be readily observed on GaP, where surface transport is kinetically limited.

Second, if surface inhomogeneity causes an uneven distribution of charge buildup within the electrode, then surface proton shuttling can also serve to quickly regulate and offset the resulting potential difference. Such a potential difference could result from one surface region becoming rich in charged dangling-bond states or component semiconductor atoms with an altered oxidation state. Placed in the context of surface corrosion resistance, this means that a surface protonic current (Figure 6c) may be able to replace a corrosion-inducing electronic current (Figure 6d), thereby stabilizing the surface.

We can illustrate this more specifically in the case of *p*-InP, for which photocorrosion in the absence of an oxide layer is thought to occur via a two-step process.[55,67] The first step is a cathodic process involving the release of PH_3, which causes In^0 metal to inhomogeneously agglomerate at the surface. In a subsequent anodic process (driven by photogenerated holes or by the resulting surface potential difference), the surface In^0 is oxidized to In^{3+} and dissolved. According to our results, the presence of a thin surface oxide would hydroxylate the surface and enable fast proton shuttling on InP(001). This could offset the surface potential difference with protons in lieu of electrons and holes, thereby arresting corrosion. The competing processes are illustrated in c and d of Figure 6.

Third, our simulations suggest that GaP(001) is energetically much more likely to have exposed surface *M*−O−*M* oxygen bridges than InP(001) (Table 1). Strained oxygen bridges lead to hole traps and recombination sites under illumination, and have been proposed as possible nucleation sites for photocorrosion.[19] Although this mechanism has yet to be verified experimentally, it suggests that higher native concentrations of exposed oxygen bridges at the GaP(001)−water interface would correspond directly to higher corrosivity. It also means that environments that facilitate protonation of surface oxygen bridges should exhibit improved passivation, which may

contribute to reported improvements in corrosion resistance in acidic electrolytes.[51,54,62]

Because corrosion mitigation remains a goal for the development of reliable III−V semiconductor photocathodes, we can use our insights to propose a basic criterion for maintaining surface integrity. In particular, the formation of a fluid hydrogen-bond network with the capability for long-range hydrogen transport should be prioritized. This provides a mechanism for self-healing of surface imperfections and potential differences. However, in tuning the surface chemistry, one also needs to consider the trade-off between the strength of the interfacial hydrogen-bond network and that of the interfacial O−H chemical bonds. Since favorable kinetics for local proton transfer and network reorganization are both necessary for long-range transport, there should be an ideal window of intermediate interfacial hydrogen and chemical bond strengths that should be targeted by electrolyte or electrode surface engineering.

Finally, if strained oxygen bridges are nucleation sites for surface decomposition under illumination, then we could use chemically or mechanically induced local surface compression for surface stabilization. Lattice strain may be an underlying contributor to the higher corrosivity of $GaInP_2$ compared to GaP,[11] since the larger lattice constant of $GaInP_2$ with respect to GaP would generally induce local tensile strain in surface Ga−O bonds. This hypothesis could be tested by changing the growth substrate to compress the surface, for instance. One might also accept the presence of oxygen bridges but ensure the grown oxide is sufficiently uniform and defect free so as to prevent buildup of any strain or potential differences that lead to corrosion.

CONCLUSIONS

In conclusion, we have used *ab initio* molecular dynamics simulations to investigate how the properties of water are modified at the interface with natively hydroxylated InP(001) and GaP(001). For both surfaces, the interface is stabilized by strong hydrogen bonding with water, causing formation of an ice-like structure in which proton hopping is enhanced. Despite similar electronic structures, InP and GaP exhibit fundamentally different interfacial structure and dynamics. For InP(001), the water hydrogen-bond network is significantly more fluid, which permits facile topological reorganization in a way inaccessible to GaP(001). Accordingly, local proton hopping can give rise to rapid long-range surface shuttling of hydrogen. This same shuttling is kinetically unfavorable for GaP(001) due to the relative stiffness of its hydrogen-bond network. The significant differences between the two surfaces turn out to be an unexpected consequence of slightly more covalent-like character in the Ga−O surface bonds.

The possibility of long-range surface hydrogen transport at the InP(001)−water interface activates additional mechanisms in which different stages of multistage surface reactions can be spatially separated. This makes additional surface reaction sites available for both hydrogen evolution and corrosion mitigation. Accordingly, fast surface hydrogen transport may enhance hydrogen evolution by permitting the proton adsorption and H_2 desorption steps to be physically separated (e.g., on the InP surface and Pt catalyst). In the case of the corrosion reaction, this same surface transport may contribute to the corrosion resistance of surface-oxidized InP by allowing for rapid passivation of dangling bonds and offset of surface potential differences that need not be local to the adsorption site. We show that in several instances, the possibility of spatially separated reaction stages is consistent with experimental observations.

In light of our models, we suggest some broad strategies for enhanced hydrogen evolution and mitigation of surface corrosion. These include the deliberate formation of a surface hydrogen-bond network with properly tuned binding strength; the engineering of chemically or mechanically induced local compressive lattice strain; and the intentional growth of a carefully controlled surface oxide with minimal defects. We hope that these suggestions will aid future efforts toward improved durability and performance of III−V-based photoelectrodes. We point out that using surface transport to enable mechanisms in which components of a multistep reaction can be spatially separated allows the component reactions to be independently tuned. This could open up additional engineering possibilities for electrocatalytic and photocatalytic devices.

ASSOCIATED CONTENT

Supporting Information

This material is available free of charge via the Internet at http://pubs.acs.org.

AUTHOR INFORMATION

Corresponding Author

brandonwood@llnl.gov

Notes

The authors declare no competing financial interest.

ACKNOWLEDGMENTS

We acknowledge helpful discussions with J. Turner, T. Deutsch, and H. Wang (NREL), and with D. Esposito (NIST). Funding was provided by the U.S. Department of Energy Fuel Cell Technologies Program. Computing support came from the Lawrence Livermore National Laboratory (LLNL) Institutional Computing Grand Challenge program. This work was performed under the auspices of the U.S. Department of Energy by LLNL under Contract DE-AC52-07NA27344.

REFERENCES

(1) U.S. Department of Energy, DOE Basic Energy Sciences Advisory Committee (BESAC) Report: *New Science for a Secure and Sustainable Energy Future*, http://science.energy.gov/~/media/bes/pdf/reports/files/nsssef_rpt.pdf, 2008.
(2) Fujishima, A.; Honda, K. *Nature* **1972**, *238*, 37.
(3) Lewis, N. S.; Nocera, D. G. *Proc. Natl. Acad. Sci. U.S.A.* **2006**, *103*, 15729.
(4) Turner, J.; et al. *Int. J. Energy Res.* **2008**, *32*, 379.
(5) Khaselev, O.; Turner, J. A. *Science* **1998**, *280*, 425.
(6) Menezes, S.; Miller, B.; Bachmann, K. J. *J. Vac. Sci. Technol. B* **1983**, *1*, 48.
(7) Lewerenz, H.; Schulte, K. *Electrochim. Acta* **2002**, *47*, 2639 − 2651.
(8) Vigneron, J.; Herlem, M.; Khoumri, E. M.; Etcheberry, A. *Appl. Surf. Sci.* **2002**, *201*, 51.
(9) Wang, H.; Turner, J. A. *ECS Trans.* **2007**, *2*, 125−133.
(10) Deutsch, T. G.; Koval, C. A.; Turner, J. A. *J. Phys. Chem. B* **2006**, *110*, 25297.
(11) Deutsch, T. G.; Head, J. L.; Turner, J. A. *J. Electrochem. Soc.* **2008**, *155*, B903−B907.
(12) Pluchery, O.; Chabal, Y. J.; Opila, R. L. *J. Appl. Phys.* **2003**, *94*, 2707−2715.
(13) Morota, H.; Adachi, S. *J. Appl. Phys.* **2006**, *100*, 054904.

(14) Kaiser, B.; Fertig, D.; Ziegler, J.; Klett, J.; Hoch, S.; Jaegermann, W. *Chem. Phys. Chem.* **2012**, *13*, 3053−3060.
(15) Heller, A. *Science* **1984**, *223*, 1141.
(16) Spicer, W. E.; Lindau, I.; Skeath, P.; Su, C. Y.; Chye, P. *Phys. Rev. Lett.* **1980**, *44*, 420−423.
(17) Lewerenz, H. J.; Aspnes, D. E.; Miller, B.; Malm, D. L.; Heller, A. *J. Am. Chem. Soc.* **1982**, *104*, 3325−3329.
(18) Chen, G.; Visbeck, S. B.; Law, D. C.; Hicks, R. F. *J. Appl. Phys.* **2002**, *91*, 9362.
(19) Wood, B. C.; Ogitsu, T.; Schwegler, E. *J. Chem. Phys.* **2012**, *136*, 064705.
(20) Wood, B. C.; Ogitsu, T.; Schwegler, E. *J. Photon. Energy* **2011**, *1*, 016002.
(21) Wood, B. C.; Schwegler, E.; Choi, W.-I.; Ogitsu, T. *J. Phys. Chem. C*, submitted.
(22) May, M. M.; Supplie, O.; Höhn, C.; van de Krol, R.; Lewerenz, H.-J.; Hannappel, T. *New J. Phys.* **2013**, *15*, 103003.
(23) Car, R.; Parrinello, M. *Phys. Rev. Lett.* **1985**, *55*, 2471.
(24) Giannozzi, P.; et al. *J. Phys.: Condens. Matter* **2009**, *21*, 395502.
(25) Vanderbilt, D. *Phys. Rev. B* **1990**, *41*, 7892.
(26) Perdew, J. P.; Burke, K.; Ernzerhof, M. *Phys. Rev. Lett.* **1996**, *77*, 3865.
(27) Zhao, Y.; Truhlar, D. G. *J. Chem. Theory Comput.* **2005**, *1*, 415−432.
(28) Marx, D. *ChemPhysChem* **2006**, *7*, 1848−1870.
(29) Hass, K. C.; Schneider, W. F.; Curioni, A.; Andreoni, W. *Science* **1998**, *282*, 265−268.
(30) Li, S.-C.; Zhang, Z.; Sheppard, D.; Kay, B. D.; White, J. M.; Du, Y.; Lyubinetsky, I.; Henkelman, G.; Dohnálek, Z. *J. Am. Chem. Soc.* **2008**, *130*, 9080−9088.
(31) Kato, H. S.; Akagi, K.; Tsuneyuki, S.; Kawai, M. *J. Phys. Chem. C* **2008**, *112*, 12879−12886.
(32) Cicero, G.; Galli, G.; Catellani, A. *J. Phys. Chem. B* **2004**, *108*, 16518−16524.
(33) Wang, J.; Pedroza, L. S.; Poissier, A.; Fernandez-Serra, M. V. *J. Phys. Chem. C* **2012**, *116*, 14382−14389.
(34) Sun, C.; Liu, L.-M.; Selloni, A.; Lu, G. Q. M.; Smith, S. C. *J. Mater. Chem.* **2010**, *20*, 10319−10334.
(35) Meng, S.; Wang, E. G.; Gao, S. *Phys. Rev. B* **2004**, *69*, 195404.
(36) Carrasco, J.; Hodgson, A.; Michaelides, A. *Nat. Mater.* **2012**, *11*, 667−674.
(37) Muñoz García, A. B.; Carter, E. A. *J. Am. Chem. Soc.* **2012**, *134*, 13600−13603.
(38) Merte, L. R.; Peng, G.; Bechstein, R.; Riebolt, F.; Farberow, C. A.; Grabow, L. C.; Kudernatsch, W.; Wendt, S.; Lægsgaard, E.; Mavrikakis, M.; Besenbacher, F. *Science* **2012**, *336*, 889 −893.
(39) Cicero, G.; Grossman, J. C.; Catellani, A.; Galli, G. *J. Am. Chem. Soc.* **2005**, *127*, 6830−6835.
(40) Sumita, M.; Hu, C.; Tateyama, Y. *J. Phys. Chem. C* **2010**, *114*, 18529−18537.
(41) Wood, B. C.; Marzari, N. *Phys. Rev. B* **2007**, *76*, 134301.
(42) Jost, L. *Oikos* **2006**, *113*, 363−375.
(43) Vittadini, A.; Selloni, A.; Rotzinger, F. P.; Grätzel, M. *Phys. Rev. Lett.* **1998**, *81*, 2954−2957.
(44) Lockwood, G. K.; Garofalini, S. H. *J. Chem. Phys.* **2009**, *131*, 074703.
(45) Shen, X.; Small, Y. A.; Wang, J.; Allen, P. B.; Fernandez-Serra, M. V.; Hybertsen, M. S.; Muckerman, J. T. *J. Phys. Chem. C* **2010**, *114*, 13695−13704.
(46) Nogami, M.; Abe, Y. *Phys. Rev. B* **1997**, *55*, 12108−12112.
(47) Nogami, M.; Nagao, R.; Wong, C. *J. Phys. Chem. B* **1998**, *102*, 5772−5775.
(48) Bockris, J. O.; Khan, S. U. M. *Surface Electrochemistry: A Molecular Level Approach*; Plenum Press: New York, 1993.
(49) Chazalviel, J.-N.; Belaïdi, A.; Safi, M.; Maroun, F.; Erné, B. H.; Ozanam, F. *Electrochim. Acta* **2000**, *45*, 3205 −3211.
(50) Li, Y.; Wang, H.; Xie, L.; Liang, Y.; Hong, G.; Dai, H. *J. Am. Chem. Soc.* **2011**, *133*, 7296−7299.
(51) Heller, A.; Aharon-Shalom, E.; Bonner, W. A.; Miller, B. *J. Am. Chem. Soc.* **1982**, *104*, 6942−6948.
(52) Butler, M. A.; Ginley, D. S. *Appl. Phys. Lett.* **1983**, *42*, 582−584.
(53) Szklarczyk, M.; Bockris, J. O. *J. Phys. Chem.* **1984**, *88*, 5241−5245.
(54) Bansal, A.; Turner, J. A. *J. Phys. Chem. B* **2000**, *104*, 6591−6598.
(55) Bogdanoff, P.; Friebe, P.; Alonso-Vante, N. *J. Electrochem. Soc.* **1998**, *145*, 576−582.
(56) Appleby, A. J.; Chemla, M.; Kita, H.; Bronoël, G. In *Encyclopedia of the Electrochemistry of the Elements, Vol. IXA*; Bard, A. J., Ed.; Marcel Dekker, New York, 1982.
(57) Marković, N. M.; Grgur, B. N.; Ross, P. N. *J. Phys. Chem. B* **1997**, *101*, 5405−5413.
(58) Kühne, H.-M.; Schefold, J. *J. Electrochem. Soc.* **1990**, *137*, 568−575.
(59) Esposito, D. V.; Levin, I.; Moffat, T. P.; Talin, A. A. *Nat. Mater.* **2013**, *12*, 562−568.
(60) Szklarczyk, M.; Bockris, J. O.; Brusic, V.; Sparrow, G. *Int. J. Hydrogen Energy* **1984**, *9*, 707−715.
(61) Conway, B.; Tilak, B. *Electrochim. Acta* **2002**, *47*, 3571 −3594.
(62) Khaselev, O.; Turner, J. A. *J. Electrochem. Soc.* **1998**, *145*, 3335−3339.
(63) Aspnes, D. E.; Heller, A. *J. Phys. Chem.* **1983**, *87*, 4919−4929.
(64) Heller, A. *J. Phys. Chem.* **1985**, *89*, 2962−2963.
(65) Menezes, S.; Lewerenz, H. J.; Thiel, F. A.; Bachmann, K. J. *Appl. Phys. Lett.* **1981**, *38*, 710−712.
(66) Heller, A.; Miller, B.; Lewerenz, H. J.; Bachmann, K. J. *J. Am. Chem. Soc.* **1980**, *102*, 6555.
(67) Schulte, K. H.; Lewerenz, H. J. *Electrochim. Acta* **2002**, *47*, 2633−2638.